ACS OMEGA

http://pubs.acs.org/journal/acsodf

Article

Ionic Liquids Endowed with Novel Hybrid Anions for Supercapacitors

Wenjie Xiong, Zengyu Yin, Xiaomin Zhang,* Zhuoheng Tu, Xingbang Hu, and Youting Wu*

Cite This: *ACS Omega* 2022, 7, 26368−26374

Read Online

ACCESS | Metrics & More | Article Recommendations | Supporting Information

ABSTRACT: The synthesis of a novel class of ionic liquids (ILs) with sulfimide-type anions is presented herein. [Py_{14}][PTSNTF] (*N*-butyl-*N*-methylpyrrolidinium *p*-tosyl(trifluoromethyl)sulfonimide) shows that the maximal electrochemical window is as high as 5.3 V, higher than that of most reported ILs. In addition, thermogravimetry analysis, differential scanning calorimetry, and the flammability test were also carried out for its thermal stability and practical safety. Impressively, these ILs exhibited good flame resistance and demonstrated an admirable intrinsic safety, in sharp contrast to ordinary electrolytes. Furthermore, the electrostatic potential of ILs was calculated theoretically, and the distribution of surrounding charge is intuitively understood. Cyclic voltammetry, galvanostatic charge−discharge tests, and cycling stability measurement were performed to evaluate the potential as the electrolyte for supercapacitors. The insights obtained from the study of novel anions provide new ideas for the design of novel IL electrolytes for energy applications.

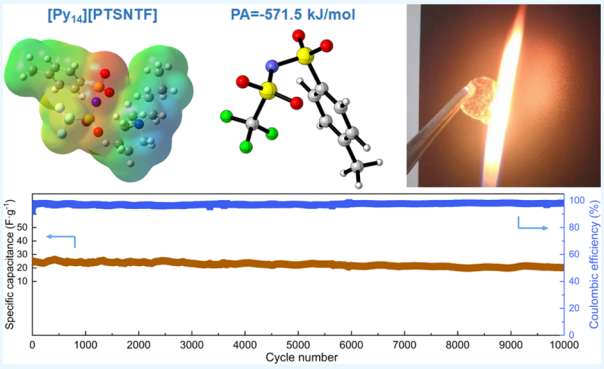

1. INTRODUCTION

Development of the use of chemical energy storage under the condition of a short pulse is of interest because time is dependent on the power output. Electrochemical double-layer capacitors (EDLCs), also known as supercapacitors, have received much attention because of their high power density, low operating cost, and good stability upon cycling, which is a potential application as the pulse power supply for such digital devices and electric vehicles. The traditional EDLCs consist of activated carbon-based electrodes, an insulated separator, and organic electrolytes. Conventional electrolytes such as aqueous (e.g., NH_4Cl, KOH, H_2SO_4, etc.) and various nonaqueous liquid electrolytes (such as acetonitrile or propylene carbonate) are available in commercial EDLCs.[1−4] However, there are still several disadvantages, including fluid leakage, high flammability, toxicity, and corrosivity, which have limited the application of EDLCs at higher operating temperatures.

Ionic liquids (ILs), as a state-of-the-art kind of ambient temperature molten salt, have captured intensive insights because of their green characteristic. Close attention to the ILs has been widely paid in various aspects, such as electrolytes,[5−7] energy applications,[8−10] catalytic reactions,[11,12] material modifications,[13,14] and efficient gas absorbents.[15−17] Compared with the traditional organic electrolytes, they are considered to be more secure because of their negligible vapor pressure, high thermal stability, and nonflammability, which have therefore been considered as a substitute for organic electrolytes in EDLCs. The cations and anions do not match in terms of size and tend to exhibit some degree of charge delocalization due to the weak interaction between the constituent ions, which is usually responsible for their high ionic conductivity. Rennie et al. disclosed a series of trialkyl sulfonium cations (S-ILs) coupled with the bis-(trifluoromethanesulfonyl)imide anion ([S_{22x}][TFSI]).[18] The electrochemical windows of these ILs are no more than 3.8 V at 298 K. In addition, the thermal decomposition temperatures of [S_{22x}][Tf_2N] are located below 573 K, and their flame resistance needs to be further studied. Gunderson-Briggs and co-workers reported an IL with the hybrid anion of triflamide and carbonate.[19] The thermal decomposition temperature of [C_4mpyr][MCTFSI] (*N*-butyl-*N*-methyl pyrrolidinium methylcarbonate(trifluoromethylsulfonyl)imide) is 543 K from thermogravimetric analysis (TGA). Essentially, the structure of anions is innovative and presents a potential application prospect in electrochemistry. Varela et al. synthesized a series of piperidinium-based ILs paired with the [TFSI] anion as the electrolyte for supercapacitors with large electrochemical windows and high thermal stability.[20] Pohlmann investigated the application of azepanium cations paired with the [TFSI] anion as the electrolyte for EDLCs with

Received: April 8, 2022
Accepted: July 6, 2022
Published: July 18, 2022

the melting point up to 298 K, which limits the scope of use from the point of temperature.[21] Martins et al. reported the application of ILs containing tetracyanoborate anions ([B(CN)$_4$]) thanks to their wide operating potential for supercapacitors.[22] A series of reviewers discuss the advantages of the application of ILs or IL-mixture-based electrolytes for supercapacitors.[23−26] Overall, the reported ILs for EDLCs are usually based on symmetric [TFSI], [FSI], [B(CN)$_4$], and so on. Developing other novel types of hybrid ILs to correlate the structure−property relationship is of importance for application in EDLCs.

Herein, a novel kind of hybrid anion consisting of trifluoromethylsulfonyl and *p*-tosylsulfonyl was designed and prepared. As the expansion of the novel hybrid sulfimide-type IL electrolytes, this paper mainly introduces its synthesis steps, physicochemical, and electrochemical properties, including density, viscosity, electrochemical stability window, and ionic conductivity, thermogravimetry-differential scanning calorimetry (TG-DSC), flammability test, and theoretical calculations. The electrochemical performance of commercial carbon-based symmetric supercapacitors based on these ILs was evaluated by cyclic voltammetry (CV), galvanostatic charge−discharge (GCD), and cycling stability tests. It is believed that the hybrid one can give readers an idea to design novel electrolytes in future and extends the approach of ILs in the field of electrolytes for supercapacitors.

2. EXPERIMENTAL SECTION

2.1. Materials. The specifications and sources of the chemicals used in this work are summarized in Table S1. All reagents were used as received without further purification.

2.2. Preparation and Characterization. The chemical structures are shown in Scheme 1, and the basic physicochemical properties have been further investigated. For a typical run, the synthesis of the sodium salt of *p*-tosyl(trifluoromethylsulfonyl)imide (Na[PTSNTF]), *N*-butyl-*N*-methyl pyrrolidinium bromide ($Py_{14}Br$), and *N*-butyl-*N*-methyl pyrrolidinium *p*-tosyl(trifluoromethylsulfonyl)imide ([Py_{14}][PTSNTF]) was carried out according to Scheme 2.

Scheme 1. Chemical Structure of ILs Used in This Study

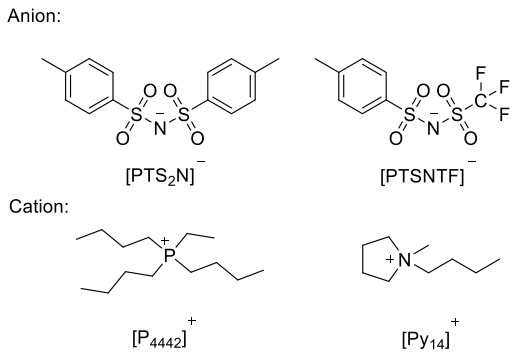

2.2.1. Synthesis of Na[PTSNTF]. The starting material *p*-toluenesulfonamide (1.0 equiv) and NaH (2.0 equiv) were added to a flask with tetrahydrofuran under a nitrogen atmosphere. The mixture was stirred at 0 °C for 24 h. After that, it was filtered, and the filter cake was dried in a vacuum to obtain the white sodium *p*-tosylamide ($PTSNNa_2$). The obtained sodium *p*-tosylamide (1.0 equiv) and trifluoromethanesulfonyl chloride (1.3 equiv) were dissolved in dry acetonitrile at ambient temperature. The mixture was warmed to ambient temperature and mixed for 24 h. After removing the solvent with rotary evaporation, the mixture was washed two times with dry diethyl ether. Afterward, diethyl ether was removed under vacuum, and the white powder Na[PTSNTF] was obtained. Its morphology can be seen in Figure S1. The synthesis procedure of Na[PTS_2N] worked the same way.

2.2.2. Synthesis of $Py_{14}Br$. *N*-Methyl-pyrrolidine (1.0 equiv) and 1-bromobutane (1.2 equiv) were added to a flask with ethanol as the solvent and refluxed for 48 h at 343.2 K. The product was washed three times with ethyl acetate to remove the unreacted raw material, and the solvent was removed by vacuum drying for 6 h. The white powder ($Py_{14}Br$) was finally obtained.

2.2.3. Synthesis of the IL ([Py_{14}][PTSNTF]). Na[PTSNTF] (1.1 equiv) and $Py_{14}Br$ (1.0 equiv) were added to a flask with deionized water as the solvent. The mixture was stirred at ambient temperature for 24 h. Then the mixture was extracted with dichloromethane three times. After the removal of the solvent under vacuum, the viscous pale-yellow liquid [Py_{14}][PTSNTF] was obtained. The synthesis procedure of [P_{4442}][PTSNTF] worked the same way.

2.2.4. Characterization. Nuclear magnetic resonance (NMR) was performed to confirm the chemical structures of these four ILs. The NMR spectrum was obtained on a Bruker DPX 400 MHz spectrometer with $CDCl_3$ as the standard solvent. Thermal stability was determined using TGA under an N_2 atmosphere at a scanning rate of 10 K·min^{-1} to explore the decomposition temperature of ILs. DSC was carried out using a Mettler Toledo DSC1 with liquid nitrogen cooling. Samples were heated under a nitrogen atmosphere from 193.2 to 303.2 K at a rate of 10 K·min^{-1} to explore the melting point (T_m) of ILs. Densities and viscosities were measured on an Anton Paar DMA 5000 type automatic densitometer with a precision of 0.0001 g/cm^3 and a Brookfield LVDV-II + Pro viscometer with an uncertainty of ±1%, respectively. Linear sweep voltammetry (LSV) was performed on a CHI760E electrochemical workstation. Glassy carbon (GC), a platinum wire, and the Ag/AgCl electrode were used as the working electrode, the

Scheme 2. Schematic Illustration of the [Py_{14}][PTSNTF] Preparation

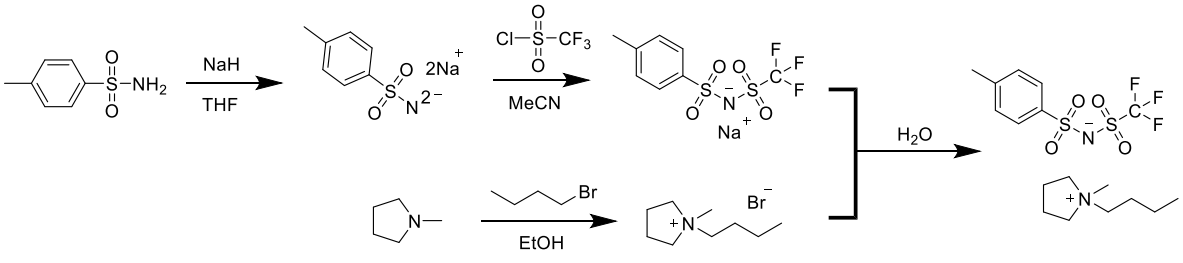

https://doi.org/10.1021/acsomega.2c02211
ACS Omega 2022, 7, 26368−26374

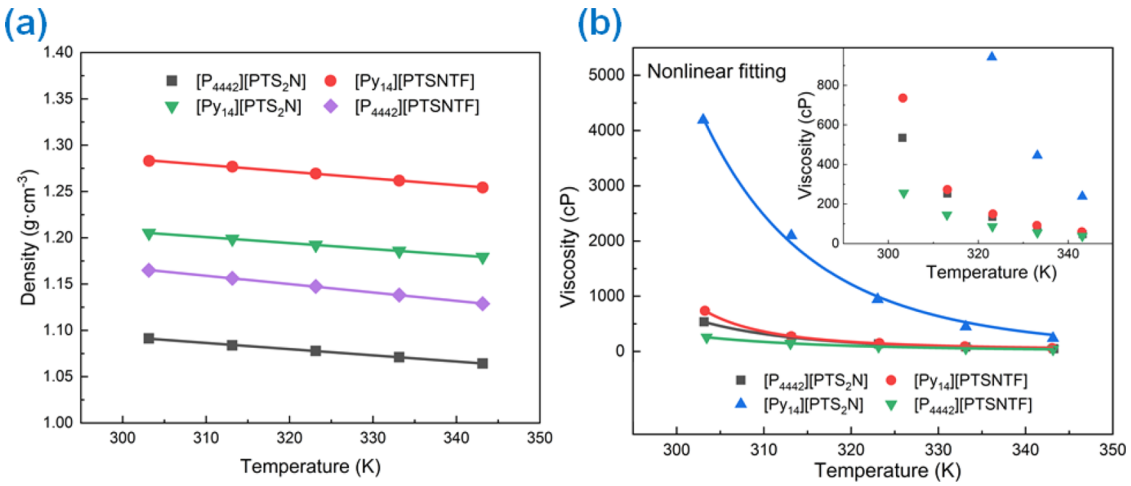

Figure 1. Experimental density (a) and viscosity (b) in a range of temperatures for these ILs in this study.

Table 1. Parameters Fitted to the Experimental Data

parameters		$[P_{4442}][PTS_2N]$	$[Py_{14}][PTS_2N]$	$[P_{4442}][PTSNTF]$	$[Py_{14}][PTSNTF]$
linear fitting	A (g cm^{-1})	1.294	1.401	1.440	1.504
	$B \times 10^4$ (g cm^{-1} K^{-1})	−6.681	−6.463	−9.070	−7.265
nonlinear fitting	η_0 (cP)	0.0559	0.0098	0.0729	0.0656
	D (K)	1034	2470	1050	1084
	T_0 (K)	190.4	143.6	174.8	264.8

counter electrode, and the reference electrode, respectively. The ILs were dried on a Schlenk line at 0.15 mbar and 60 °C for 6 h until no further bubbles' evolution was observed. Coulometric Karl Fisher titration was used to measure the water concentration of these IL samples. The water contents of $[P_{4442}][PTSNTF]$, $[Py_{14}][PTSNTF]$, $[P_{4442}][PTS_2N]$, and $[Py_{14}][PTS_2N]$ were 67, 79, 73, and 71 ppm, respectively.

2.3. Electrochemical Measurements. The ionic conductivity was determined using the impedance method at different temperatures with a frequency of 1 MHz to 1 Hz on a CHI760E electrochemical workstation. Briefly, the ILs were placed in two symmetrical stainless-steel plates separated by a porous PTFE gasket.

To evaluate the electrochemical performance of the cells, coin cell (CR2032) configurations were constructed in a glovebox with nitrogen as protecting gas. For the active carbon electrode preparation, a slurry containing Kuraray Active Carbon, PVDF, and Super P at a weight ratio of 8:1:1 using NMP as a solvent was prepared until a homogenous paste was formed. The paste was spread on an aluminum current collector, dried, and finally applied as the cathode with a diameter of 14 mm and mass loading of active materials of 1.0−1.5 mg·cm^{-2}. The separator was soaked in the desired IL, and then the cell components were placed under vacuum in the glovebox antechamber for roughly 5 min to encourage the impregnation of the electrolyte into the electrode porosity. The soaked separator was sandwiched between two electrodes in the coin cells after sufficient impregnation, which were assembled in a nitrogen glovebox with a low concentration of O_2 (<0.1 ppm) and humidity (H_2O < 0.1 ppm).

2.4. Theoretical Calculation Method. All the structures were fully optimized with the density functional theory method including the dispersion correction (B3LYP) method using the Empirical Dispersion = GD3BJ keyword. The 6-31g(d) basis set was used for all atoms (abbreviation as B3LYP/6-31g(d)). The influence of methanol solvent was investigated in the condensed phase using the polarizable continuum model at B3LYP/6-31g(d) method. Energy calculations and zero-point energy correction have been performed by using the same level of theory. All calculations were performed with the Gaussian 09 suite of programs.

3. RESULTS AND DISCUSSION

The inorganic sodium salt (Na[PTSNTF]) was analyzed by elemental analysis, and the element contents of C, H, and N were 29.2, 2.26, and 4.1%, respectively, fitting well with the theoretical value. The successful preparation of $[Py_{14}][Br]$, $[Py_{14}][PTSNTF]$, and $[P_{4442}][PTSNTF]$ was directly reflected through NMR. For comparison, symmetrical $[PTS_2N]$-based ILs were also prepared. No impurities can be found from the characterization (Figures S2−S17).

Density and viscosity are important foundational physicochemical properties required for process design. In Figure 1, linear and Vogel−Tamman−Fulcher (VTF) equations were used to approximate the density and viscosity data, respectively. The density and viscosity were well fitted with eqs 1 and 2.

$$\rho = A + BT \tag{1}$$

$$\ln \eta - \ln \eta_0 = \frac{D}{T - T_0} \tag{2}$$

where A and B are equation parameters. η_0 denotes the pre-exponential constant in the unit of cP. T is the thermodynamic temperature (K). D and T_0 are equation constants. The fitting results and related model parameters are demonstrated in Figure 1 and Table 1, respectively.

It is observed that both density and viscosity decrease with increasing temperature. The densities and viscosities of these four ILs were measured in the temperature range from 303.2 to

https://doi.org/10.1021/acsomega.2c02211
ACS Omega 2022, 7, 26368−26374

343.2 K, and the densities were located in 1.05−1.30 g/cm^3. The density of [PTSNCF]-based ILs show larger values than those of [PTS$_2$N]-based ILs, and viscosity shows the opposite tendency, demonstrating that the hybridization of trifluoromethylsulfonyl and methylphenyl in anions is favorable for the reduction of viscosity. In particular, the viscosity of [Py$_{14}$][PTSNTF] at 313.2 K is up to 273.4 cP, which indicates that it will have good fluidity as an electrolyte for any energy device[27] although it has a higher viscosity value than other imide-based ILs.[38]

Indispensably, temperature-dependent electrochemical impedance spectroscopy (EIS) measurements (Figure S18) were performed to evaluate the ionic conductivity of these ILs. Figure 2 shows the ionic conductivity of the four ILs calculated

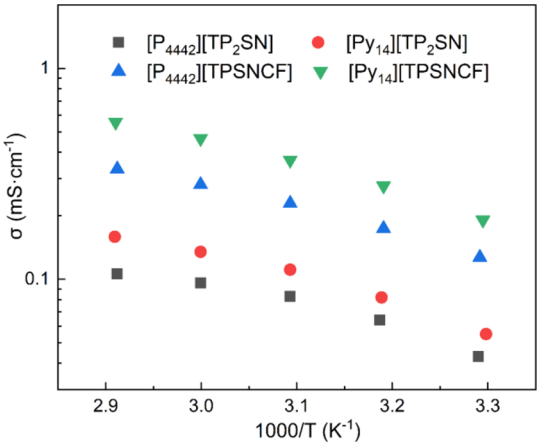

Figure 2. Ionic conductivity in a range of temperatures for these ILs in this study.

from the EIS test results as a function of temperature with eq 3. As is well established, ionic conductivity tends to increase with the increasing temperature. Similar to the viscosity fitting, the VTF equation can be used to describe the charge transport properties of such ILs. It is shown that [PTSNTF]-based hybrid ILs present higher ionic conductivity than symmetric [PTS$_2$N]-based ILs. [Py$_{14}$][PTSNTF] exhibited the highest conductivity in the four ILs, which is probably related to its low viscosity and asymmetric hybridization.[28,29] At 303 K, the ionic conductivity of [P$_{4442}$][PTS$_2$N], [P$_{4442}$][PTSNTF], [Py$_{14}$][PTS$_2$N], and [Py$_{14}$][PTSNTF] presents 0.045, 0.127, 0.053, and 0.191 mS·cm^{-1}, respectively.

$$\sigma = \frac{L}{Z \times S} \tag{3}$$

where Z is the impedance of the real axis in the Nyquist diagram, L is the thickness of the PTFE gasket, and S is the area of the hole on the PTFE gasket.

Thermal stability is another important parameter that is of significance in evaluating the quality of electrolytes. There is only one mass loss stage for each IL, demonstrating the formation of pure ILs. In Figure 3, it can be found that the thermal decomposition temperature (T_d) of [P$_{4442}$][PTS$_2$N], [P$_{4442}$][PTSNTF], [Py$_{14}$][PTS$_2$N], and [Py$_{14}$][PTSNTF] presents 635, 627, 570, and 599 K, respectively, which means that they have good temperature tolerance.

Additionally, a flammability test has been carried out. As shown in Figure 4a−c, a blank glass fiber membrane without any ILs can be easily destroyed by flame. However surprisingly,

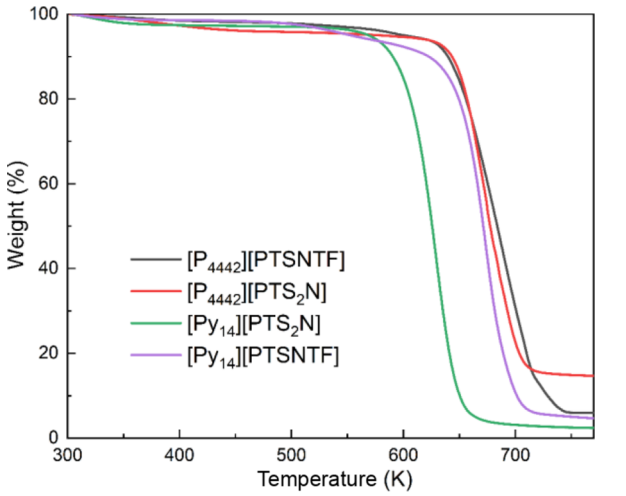

Figure 3. Thermogravimetry in a range of temperatures for these ILs in this study.

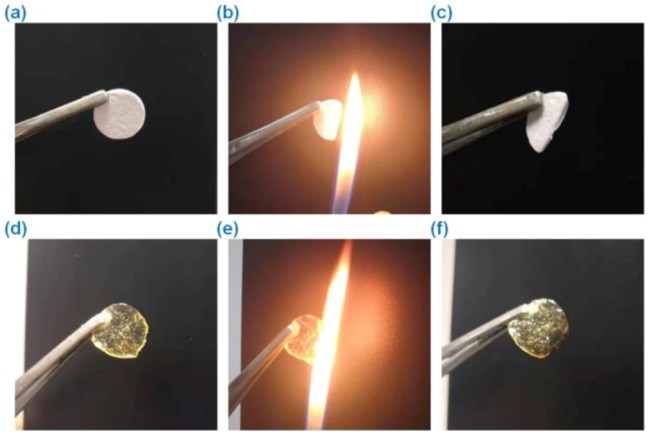

Figure 4. Flammability test of the glass fiber membrane with and without [Py$_{14}$][PTSNTF]. (a) Blank membrane; (b) blank membrane with flaming; (c) blank membrane after flaming; (d) soaked; (e) soaked with flaming; (f) soaked after flaming.

when the same operation was performed on the membrane soaked in [Py$_{14}$][PTSNTF] (Figure 4d−f), the intense heat flame produced failed to ignite, which is in sharp contrast to the organic electrolyte, indicating the admirable intrinsic safety even in the application under extreme conditions. From Figure S19, the glass transition temperatures (T_g) of [P$_{4442}$][PTS$_2$N], [P$_{4442}$][PTSNTF], [Py$_{14}$][PTS$_2$N], and [Py$_{14}$][PTSNTF] obtained by DSC are as low as 223, 211, 238, and 217 K, respectively, demonstrating wide liquid range windows of these investigated ILs. The solid−liquid phase variation behavior and short-term thermal stability of this kind of IL examined through DSC and TG detection indicate the wide liquid range and good thermal stability limit of ILs.[19]

As a well-established tool, electrostatic potential (ESP) has been recognized for understanding, predicting, and indicating the chemical reactivity of molecules and their ability to participate in some types of interactions. As shown in Figures 5a and S20, the red and blue colors on the IL surface indicate regions with more negative and positive ESPs, respectively (the darker the color, the stronger the ESP). It can be seen that the anions with sulfimide groups have strong electronegativity, while as cations, [Py$_{14}$] and [P$_{4442}$] show stable electro-

https://doi.org/10.1021/acsomega.2c02211
ACS Omega 2022, 7, 26368−26374

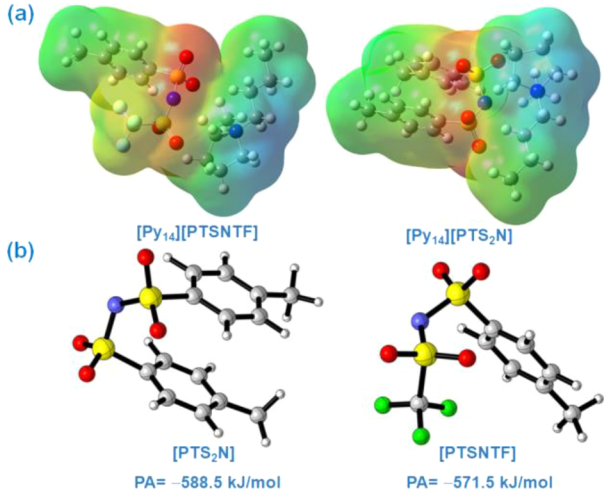

Figure 5. ESP (a) and PA (b) of [Py_{14}]-based ILs optimized at the B3LYP/6-31G(d) level.

positivity due to more alkyl chains. Compared with the symmetrical [PTS_2N], the hybrid structure of [PTSNTF] can effectively reduce the delocalization of negative charge by replacing the *p*-tosylsulfonyl group with the strong electron-withdrawing trifluoromethyl, which is conducive to the electrostatic interaction between the cation and anion.[30] Most of the strong ESP cross sections are consistent with the anions and cations of the above ILs. The Cartesian coordinates and the relevant calculations of ILs are presented in the Supporting Information. Hence, compared with the related anion structures, the proton affinities (PAs) of [PTS_2N] and [PTSNTF] were calculated (Figure 5b). The PAs are −588.5 and −571.5 kJ/mol, respectively. Like other commonly used highly charge-delocalized anions, which fell in the range of −700 to −500 kJ/mol on the proton affinity scale.[31]

To effectively evaluate the ionicity of the ILs, the Walden plot of $\log(\Lambda)$ against $\log(\eta^{-1})$ graph of these ILs (Figure 6a) calculated from density, molecular weight, viscosity, and ionic conductivity shows that the ILs all lie slightly below the ideal line, indicating that they have a low degree of pairing or aggregation type interactions and that they can therefore be considered as "good" ILs.[32−34] Obviously, hybrid [PTSNTF]-based ILs indicate more free ions to contribute the ionic conductivity in comparison with symmetric [PTS_2N]-based ILs.

To assess the electrochemical performance of these designed ILs, [Py_{14}][PTSNTF] was optimized as a representative thanks to the largest ionic conductivity and wide electrochemical window. A coin cell (CR2032) was used as the symmetrical capacitor, which consists inside of a stainless-steel spacer, a commercial carbon material (YP-50F, Kuraray) based electrode, and a glass fiber membrane (GF/A, Whatman) as the separator. The configurations of the coin cells were as follows: [Negative cover|Spacer|Electrode|[Py_{14}][PTSNTF]-soaked separator|Electrode|Spacer|Spring gasket|Positive cover]. Considering the discharge time of the cells, a wider range of charge/discharge rates and the charge/discharge curves of the symmetrical capacitor were explored using galvanostatic cycling at the specific current densities between 0.05 and 1.0 $A{\cdot}g^{-1}$, and the results are presented in Figures 6b,c. The specific capacitance of the individual capacitor was calculated from eqs 4 and 5. Through calculation, the specific capacities of the capacitor are 28.4, 24.4, 20.5, 14.1, and 7.9 $F{\cdot}g^{-1}$ at a current density of 0.05, 0.1, 0.2, 0.5, and 1.0 $A{\cdot}g^{-1}$, respectively, which is comparable or superior to those of the EDLC based on the sulfonium cation paired with the [TFSI] anion.[18,35]

$$C_{dev} = \frac{I\Delta t}{m\Delta V} \tag{4}$$

$$C_{sp} = 2C_{dev} \tag{5}$$

where C_{dev} denotes the specific capacitance ($F{\cdot}g^{-1}$) based on the whole device, I is the discharge current (A), Δt is the discharge time (s), m is the total mass of activated carbon materials based on the whole device, and the ΔV is the

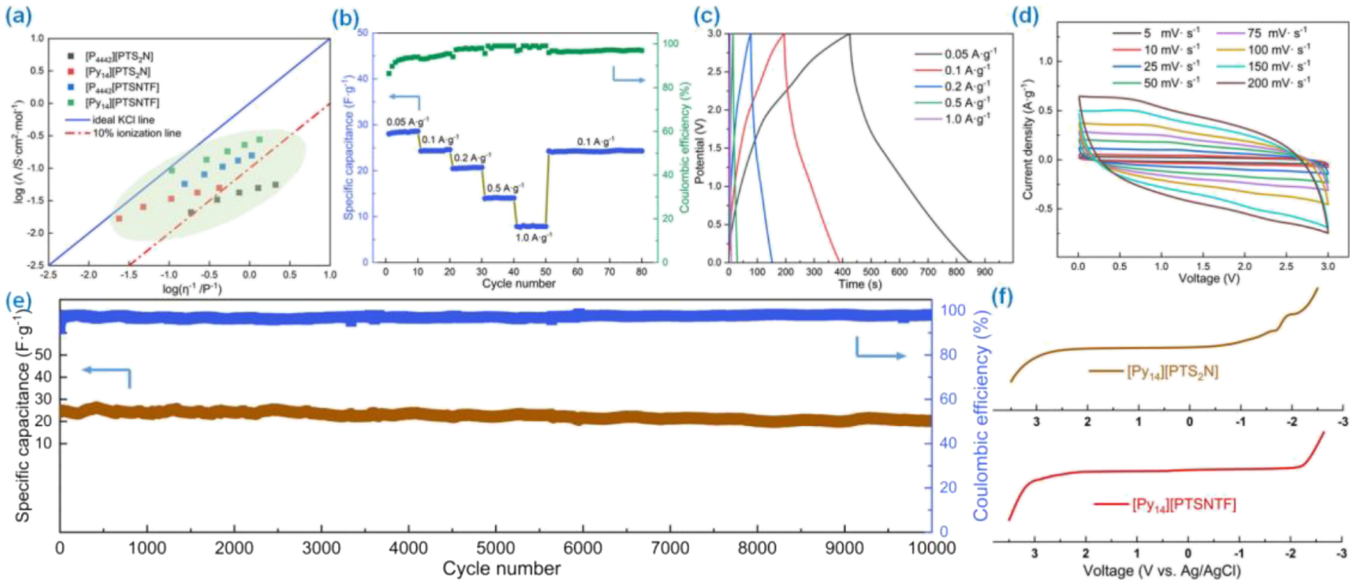

Figure 6. (a) Walden plot; (b) galvanostatic cycling plot; (c) GCD curves; (d) CV plot at different current densities; (e) cycle performance at 0.1 $A{\cdot}g^{-1}$; (f) LSV curves.

https://doi.org/10.1021/acsomega.2c02211
ACS Omega 2022, 7, 26368−26374

electrochemical window. C_{sp} denotes the specific capacitance ($F \cdot g^{-1}$) based on a single electrode.

Figure 6d shows a typical CV plot obtained for capacitors at different scan rates. It can be seen that the CV curves deviate slightly from the near-rectangular and symmetric shape, which may be due to the slow ionic transport dominated by the diffusion effect.[3] As one of the most representative peculiarities of supercapacitors, cycling stability was investigated to evaluate the performance of the EDLCs at a current density of 0.1 A g^{-1} for 10,000 cycles. As shown in Figure 6e, the retention of specific capacitance and coulombic efficiency of [Py_{14}]-[PTSNTF]-based EDLC are as high as 91.2 and 97.0% over 10,000 cycles, respectively, indicating an excellent cycling stability behavior of hybrid IL-based EDLCs.

The electrochemical window is of importance in the practical application of electrolytes. Figure 6f shows that the LSV curves were recorded at 298.2 K, showing the anode limit (AL) and cathode limit (CL) of [Py_{14}][PTS_2N] and [Py_{14}][PTSNTF] with a scan rate of 100 $mV \cdot S^{-1}$ using GC as a working electrode. For [Py_{14}][PTSNTF], it has a wide electrochemical stability window as high as 5.3 V (AL = +3.1 V and CL = −2.2 V), almost higher than that of most of those previous ILs.[36−39] The electrochemical windows of [P_{4442}]-[PTSNTF] and [P_{4442}][PTS_2N] are presented in Figure S19. It is of significance to find that [Py_{14}]-based ILs have a wider electrochemical window compared with [P_{4442}]-based ILs (for hybrid-based ILs, 5.3 V vs 2.7 V; for symmetry-based ILs, 4.2 V vs 2.8 V).

Table S2 summarizes the property of some IL electrolytes for supercapacitors. It can be seen that [Py_{14}][PTSNTF] shows a wide ESW (5.3 V) and high T_d (599 K) in comparison to other ILs. In addition, it shows conductivity values of 0.19 mS cm^{-1} at 303 K and 0.65 mS cm^{-1} at 343 K, respectively, which is higher than those of [P_{4444}][FuA], [N_{4441}][TFSI], and [P_{66614}][HOx].

4. CONCLUSIONS

In summary, we prepared two-hybrid ILs consisting of trifluoromethylsulfonyl and *p*-tosylsulfonyl. For comparison, two symmetric [PTS_2N]-based ILs were also prepared. Density, viscosity, thermal decomposition temperature, electrochemical window, and ionic conductivity were investigated systematically. The decomposition temperatures of four ILs are all above 570 K, indicating excellent thermal stability. [Py_{14}][PTSNTF] shows the largest ionic conductivity value of 0.191 mS cm^{-1} at 303.2 K, which has reached the practical application level required for supercapacitors. The electrochemical window of [Py_{14}][PTSNTF] is as high as 5.3 V, higher than those of most reported ILs. The specific capacitance of the [Py_{14}][PTSNTF]-based supercapacitor is 28.4 F g^{-1} at a current density of 0.05 A g^{-1}, which is comparable or superior to those of some reported ILs. The capacitance retention rate of the supercapacitor after 10,000 times cycling stability evaluation at a current density of 0.1 A g^{-1} is up to 91.2%, which is acceptable in energy storage devices. The coulombic efficiency remains stable at 97.0% in this charge−discharge process. It is anticipated that this work could provide alternative insight to design novel IL electrolytes for energy storage devices.

ASSOCIATED CONTENT

Supporting Information

The Supporting Information is available free of charge at https://pubs.acs.org/doi/10.1021/acsomega.2c02211.

Specifications and sources of chemicals; property comparison of ILs; image of prepared sodium salt; ^1H NMR and ^{13}C NMR spectra data of prepared ILs; EIS; DSC; LSV; and ESP; coordinates of the optimized structures (PDF)

AUTHOR INFORMATION

Corresponding Authors

Xiaomin Zhang − *Key Laboratory of Mesoscopic Chemistry of MOE, School of Chemistry and Chemical Engineering, Nanjing University, Nanjing 210023, P. R. China; Key Laboratory of Advanced Energy Materials Chemistry (Ministry of Education), College of Chemistry, Nankai University, Tianjin 300071, China;* orcid.org/0000-0002-7441-886X; Email: xmzhang@nju.edu.cn

Youting Wu − *Key Laboratory of Mesoscopic Chemistry of MOE, School of Chemistry and Chemical Engineering, Nanjing University, Nanjing 210023, P. R. China;* Email: ytwu@nju.edu.cn

Authors

Wenjie Xiong − *Key Laboratory of Mesoscopic Chemistry of MOE, School of Chemistry and Chemical Engineering, Nanjing University, Nanjing 210023, P. R. China;* orcid.org/0000-0002-6000-1692

Zengyu Yin − *Key Laboratory of Mesoscopic Chemistry of MOE, School of Chemistry and Chemical Engineering, Nanjing University, Nanjing 210023, P. R. China*

Zhuoheng Tu − *Key Laboratory of Mesoscopic Chemistry of MOE, School of Chemistry and Chemical Engineering, Nanjing University, Nanjing 210023, P. R. China*

Xingbang Hu − *Key Laboratory of Mesoscopic Chemistry of MOE, School of Chemistry and Chemical Engineering, Nanjing University, Nanjing 210023, P. R. China;* orcid.org/0000-0002-2995-9704

Complete contact information is available at: https://pubs.acs.org/10.1021/acsomega.2c02211

Notes

The authors declare no competing financial interest.

ACKNOWLEDGMENTS

This work was sponsored by the Natural Science Foundation of Jiangsu Province (BK20190310), China Postdoctoral Science Foundation (2021M691515), Foundation of Science and Technology Innovation Program of Nanjing City for Returnees from Overseas (020513006009), and the National Natural Science Foundation of China (No. 22078145). X. Zhang acknowledges the Yuxiu Young Scholars Program of Nanjing University for partial financial support.

REFERENCES

(1) Abdallah, T.; Lemordant, D.; Claude-Montigny, B. Are room temperature ionic liquids able to improve the safety of supercapacitors organic electrolytes without degrading the performances? *J. Power Sources* **2012**, *201*, 353−359.

(2) Lee, J. H.; Chae, J. S.; Jeong, J. H.; Ahn, H.-J.; Roh, K. C. An ionic liquid incorporated in a quasi-solid-state electrolyte for high-

temperature supercapacitor applications. *Chem. Commun.* **2019**, *55*, 15081−15084.
(3) Zhang, X.; Kar, M.; Mendes, T. C.; Wu, Y.; MacFarlane, D. R. Supported ionic liquid gel membrane electrolytes for flexible supercapacitors. *Adv. Energy Mater.* **2018**, *8*, No. 1702702.
(4) Sevilla, M.; Fuertes, A. B. Direct synthesis of highly porous interconnected carbon nanosheets and their application as high-performance supercapacitors. *ACS Nano* **2014**, *8*, 5069−5078.
(5) Zeng, C.; Huang, C. High-performance LiF@C-coated FeF_3·$0.33H_2O$ lithium-ion batteries with an ionic liquid electrolyte. *ACS Omega* **2022**, *7*, 688−695.
(6) Gandla, D.; Zhang, F.; Tan, D. Q. Advantage of larger interlayer spacing of a $mo_2ti_2c_3$ mxene free-standing film electrode toward an excellent performance supercapacitor in a binary ionic liquid−organic electrolyte. *ACS Omega* **2022**, *7*, 7190−7198.
(7) Domi, Y.; Usui, H.; Sugimoto, K.; Gotoh, K.; Nishikawa, K.; Sakaguchi, H. Reaction behavior of a silicide electrode with lithium in an ionic-liquid electrolyte. *ACS Omega* **2020**, *5*, 22631−22636.
(8) Mendes, T. C.; Zhang, X.; Wu, Y.; Howlett, P. C.; Forsyth, M.; Macfarlane, D. R. Supported ionic liquid gel membrane electrolytes for a safe and flexible sodium metal battery. *ACS Sustainable Chem. Eng.* **2019**, *7*, 3722−3726.
(9) Fu, J.; Xu, Y.; Dong, L.; Chen, L.; Lu, Q.; Li, M.; Zeng, X.; Dai, S.; Chen, G.; Shi, L. Multiclaw-shaped octasilsesquioxanes functionalized ionic liquids toward organic-inorganic composite electrolytes for lithium-ion batteries. *Chem. Eng. J.* **2021**, *405*, No. 126942.
(10) Xiong, W.; Tu, Z.; Yin, Z.; Zhang, X.; Hu, X.; Wu, Y. Supported ionic liquid gel membranes enhanced by ionization modification for sodium metal batteries. *ACS Sustainable Chem. Eng.* **2021**, *9*, 12100−12108.
(11) Zhang, X.; Xiong, W.; Yin, Z.; Chen, Y.; Wu, Y.; Hu, X. A novel proton-gradient-transfer acid complexes as an efficient and reusable catalyst for fatty acid esterification. *Green Energy Environ.* **2022**, *7*, 137−144.
(12) Xiong, W.; Shi, M.; Zhang, X.; Tu, Z.; Hu, X.; Wu, Y. The efficient conversion of H_2S into mercaptan alcohols mediated in protic ionic liquids under mild conditions. *Green Chem.* **2021**, *23*, 7969−7975.
(13) Dhattarwal, H. S.; Remsing, R. C.; Kashyap, H. K. How flexibility of the nanoscale solvophobic confining material promotes capillary evaporation of ionic liquids. *J. Phys. Chem. C* **2020**, *124*, 4899−4906.
(14) Fam, W.; Mansouri, J.; Li, H. Y.; Hou, J. W.; Chen, V. Effect of inorganic salt blending on the co_2 separation performance and morphology of pebax1657/ionic liquid gel membranes. *Ind. Eng. Chem. Res.* **2019**, *58*, 3304−3313.
(15) Xiong, W.; Shi, M.; Peng, L.; Zhang, X.; Hu, X.; Wu, Y. Low viscosity superbase protic ionic liquids for the highly efficient simultaneous removal of H_2S and CO_2 from CH_4. *Sep. Purif. Technol.* **2021**, *263*, No. 118417.
(16) Zhang, X.; Xiong, W.; Peng, L.; Wu, Y.; Hu, X. Highly selective absorption separation of H_2S and CO_2 from CH_4 by novel azole-based protic ionic liquids. *AIChE J.* **2020**, *66*, No. e16936.
(17) Cai, Z.; Zhang, J.; Ma, Y.; Wu, W.; Cao, Y.; Huang, K.; Jiang, L. Chelation-activated multiple-site reversible chemical absorption of ammonia in ionic liquids. *AIChE J.* **2022**, *68*, No. e17632.
(18) Rennie, A. J. R.; Martins, V. L.; Torresi, R. M.; Hall, P. J. Ionic liquids containing sulfonium cations as electrolytes for electrochemical double layer capacitors. *J. Phys. Chem. C* **2015**, *119*, 23865−23874.
(19) Gunderson-Briggs, K. E.; Rüther, T.; Best, A. S.; Kar, M.; Forsyth, C.; Izgorodiana, E. I.; MacFarlane, D. R.; Hollenkamp, A. F. A Hybrid anion for ionic liquid and battery electrolyte applications: half triflamide, half carbonate. *Angew. Chem., Int. Ed.* **2019**, *58*, 4390−4394.
(20) Varela, J. C.; Sankar, K.; Hino, A.; Lin, X. R.; Chang, W. S.; Coker, D.; Grinstaff, M. Piperidinium ionic liquids as electrolyte solvents for sustained high temperature supercapacitor operation. *Chem. Commun.* **2018**, *54*, 5590−5593.
(21) Pohlmann, S.; Olyschläger, T.; Goodrich, P.; Alvarez Vicente, J.; Jacquemin, J.; Balducci, A. Azepanium-based ionic liquids as green electrolytes for high voltage supercapacitors. *J. Power Sources* **2015**, *273*, 931−936.
(22) Martins, V. L.; Rennie, A. J. R.; Sanchez-Ramirez, N.; Torresi, R. M.; Hall, P. J. Improved performance of ionic liquid supercapacitors by using tetracyanoborate anions. *ChemElectroChem* **2018**, *5*, 598−604.
(23) Miao, L.; Song, Z.; Zhu, D.; Li, L.; Gan, L.; Liu, M. Ionic liquids for supercapacitive energy storage: a mini-review. *Energy Fuels* **2021**, *35*, 8443−8455.
(24) Eftekhari, A. Supercapacitors utilising ionic liquids. *Energy Storage Mater.* **2017**, *9*, 47−69.
(25) Yin, L.; Li, S.; Liu, X.; Yan, T. Ionic liquid electrolytes in electric double layer capacitors. *Sci. China Mater.* **2019**, *62*, 1537−1555.
(26) Feng, J.; Wang, Y.; Xu, Y.; Sun, Y.; Tang, Y.; Yan, X. Ion regulation of ionic liquid electrolytes for supercapacitors. *Energy Environ. Sci.* **2021**, *14*, 2859−2882.
(27) MacFarlane, D. R.; Sun, J.; Golding, J.; Meakin, P.; Forsyth, M. High conductivity molten salts based on the imide ion. *Electrochim. Acta* **2000**, *45*, 1271−1278.
(28) Fang, S.; Yang, L.; Wei, C.; Peng, C.; Tachibana, K.; Kamijima, K. Low-viscosity and low-melting point asymmetric trialkylsulfonium based ionic liquids as potential electrolytes. *Electrochem. Commun.* **2007**, *9*, 2696−2702.
(29) Hajime, M.; Naohiro, T.; Tatsuya, U.; Seiji, T.; Hikari, S.; Kinji, A.; Kuniaki, T. Low melting and electrochemically stable ionic liquids based on asymmetric fluorosulfonyl(trifluoromethylsulfonyl)amide. *Chem. Lett.* **2008**, *37*, 1020−1021.
(30) Liu, X.; O'Harra, K. E.; Bara, J. E.; Turner, C. H. Screening ionic liquids based on ionic volume and electrostatic potential analyses. *J. Phys. Chem. B* **2021**, *125*, 3653−3664.
(31) Izgorodina, E. I.; Forsyth, M.; MacFarlane, D. R. Towards a better understanding of delocalized charge in ionic liquid anions. *Aust. J. Chem.* **2007**, *60*, 15−20.
(32) Kang, C. S. M.; Zhang, X.; MacFarlane, D. R. Synthesis and physicochemical properties of fluorinated ionic liquids with high nitrogen gas solubility. *J. Phys. Chem. C* **2018**, *122*, 24550−24558.
(33) Yuan, W.-L.; Yang, X.; He, L.; Xue, Y.; Qin, S.; Tao, G.-H. Viscosity, conductivity, and electrochemical property of dicyanamide ionic liquids. *Front. Chem.* **2018**, *6*, 59.
(34) Xu, W.; Angell, C. A. Solvent-free electrolytes with aqueous solution-like conductivities. *Science* **2003**, *302*, 422−425.
(35) Martins, V. L.; Torresi, R. M. Ionic liquids in electrochemical energy storage. *Curr. Opin. Electrochem.* **2018**, *9*, 26−32.
(36) Hayyan, M.; Mjalli, F. S.; Hashim, M. A.; AlNashef, I. M.; Mei, T. X. Investigating the electrochemical windows of ionic liquids. *J. Ind. Eng. Chem.* **2013**, *19*, 106−112.
(37) Matsumoto, H.; Sakaebe, H.; Tatsumi, K. Preparation of room temperature ionic liquids based on aliphatic onium cations and asymmetric amide anions and their electrochemical properties as a lithium battery electrolyte. *J. Power Sources* **2005**, *146*, 45−50.
(38) Galiński, M.; Lewandowski, A.; Stępniak, I. Ionic liquids as electrolytes. *Electrochim. Acta* **2006**, *51*, 5567−5580.
(39) Shahzad, S.; Shah, A.; Kowsari, E.; Iftikhar, F. J.; Nawab, A.; Piro, B.; Akhter, M. S.; Rana, U. A.; Zou, Y. Ionic liquids as environmentally benign electrolytes for high-performance supercapacitors. *Glob. Chall.* **2019**, *3*, No. 1800023.

https://doi.org/10.1021/acsomega.2c02211
ACS Omega 2022, 7, 26368−26374